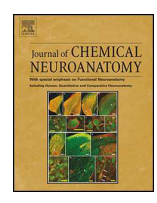
ELSEVIER

Contents lists available at ScienceDirect

Journal of Chemical Neuroanatomy

journal homepage: www.elsevier.com/locate/jchemneu



Unbiased estimation of cell number using the automatic optical fractionator



Peter R. Mouton^{a,b,c,*}, Hady Ahmady Phoulady^c, Dmitry Goldgof^c, Lawrence O. Hall^c, Marcia Gordon^b, David Morgan^b

- a Department of Pathology & Cell Biology, University of South Florida Colleges of Medicine and Engineering, 4001 E Fletcher Ave, Tampa, FL, 33613, USA
- ^b Byrd Alzheimer's Institute, University of South Florida College of Medicine, 4001 E Fletcher Ave, Tampa, FL, 33613, USA
- C Department of Computer Sciences and Engineering, College of Engineering, University of South Florida, 4202 E Fowler Ave, Tampa, FL, 33620, USA

ARTICLE INFO

Article history: Received 8 October 2016 Received in revised form 8 December 2016 Accepted 10 December 2016 Available online 14 December 2016

Keywords:
Automatic stereology
Automatic optical fractionator
Automatic disector
Automatic cell counting
Neurostereology
Optical fractionator
Automatic fractionator

ABSTRACT

A novel stereology approach, the automatic optical fractionator, is presented for obtaining unbiased and efficient estimates of the number of cells in tissue sections. Used in combination with existing segmentation algorithms and ordinary immunostaining methods, automatic estimates of cell number are obtainable from extended depth of field images built from three-dimensional volumes of tissue (disector stacks). The automatic optical fractionator is more accurate, 100% objective and 8–10 times faster than the manual optical fractionator. An example of the automatic fractionator is provided for counts of immunostained neurons in neocortex of a genetically modified mouse model of neuro-degeneration. Evidence is presented for the often overlooked prerequisite that accurate counting by the optical fractionator requires a thin focal plane generated by a high optical resolution lens.

© 2016 Elsevier B.V. All rights reserved.

1. Introduction

The accurate determination of stereology parameters for cells, nuclei, fibers and other biological objects using information from tissue sections is a well-known problem in the natural sciences. The primary theoretical obstacle is that a two-dimensional (2-D) sampling probe (knife blade) samples arbitrary-shape 3-D particles (cells) with an unknown and unknowable probability related to the cell's size, shape, and orientation on tissue sections (Wicksell, 1925). Use of the disector, a virtual 3-D probe, is the only known approach to make accurate estimates of the total cell number in tissue sections without any assumptions about the geometric properties of the cells (Sterio, 1984). The optical fractionator is an unbiased and efficient derivative of the disector method for estimating total cell number in a known fraction of the total reference volume (West et al., 1991).

Here we propose an entirely novel disector-based approach for making automatic, unbiased and efficient estimates of the number of immunostained cells in an anatomically defined reference volume. The method uses a novel combination of two recent advancements in the field of computer science: extended depth of field (EDF) images that represent 3-D neurons in a disector volume at their optimal plane of focus on a 2-D image (Valdecasas et al., 2001; Bradley and Bamford, 2004; Phoulady et al., 2015, 2016a, 2016b); and a combination of segmentation algorithms to automatically count cells visualized by ordinary staining methods in the EDF image. The main innovation lies in the automatic counting of cells in disector volumes that represent a known fraction of the reference space, hence the designation automatic optical fractionator. The automatic optical fractionator is 100% objective and therefore not subject to human errors that reduces accuracy by false negatives from overlapping cells, false positives from cells touching exclusion planes, inter-rater bias, recognition errors and user fatigue. A practical example is given for counting the total numbers of NeuN-immunostained neurons (Total N_{Neu}) in neocortex of a genetically modified mouse model of cognitive impairment and neurodegeneration.

scientist.dave@gmail.com (D. Morgan).

^{*} Corresponding author at: Department of Pathology & Cell Biology, University of South Florida College of Medicine, 4001 E Fletcher Ave, Tampa, FL, 33613, USA. *E-mail addresses*: pmouton@health.usf.edu (P.R. Mouton), parham.ap@gmail.com (H.A. Phoulady), goldgof@gmail.com (D. Goldgof), hall@cse.usf.edu (L.O. Hall), mgordon@health.usf.edu (M. Gordon),

2. Materials and methods

All procedures for animal handling and use were approved by the USF Institutional Animal Care and Use Committee and followed NIH guidelines for the care and use of laboratory animals. To validate the automatic framework for counting NeuN-immunostained neurons, this study used the well-characterized Tg4510 line with responder and activator transgenes that drive expression of a P301L tau mutation under control of a tetracycline operonresponsive element (SantaCruz et al., 2005). Tg4510 mice express mutant tau that leads to progressive cognitive decline in parallel with neuron loss and activation of neuroglia cells. Age- and sexmatched non-tg littermate control mice were included to test the automatic framework on normal (non-degenerating) neurons. Rather than test specific hypotheses related to tauopathies, neurodegeneration or neuroinflammation, these genetically modified mice and controls were selected to show a wide range of normal, neurodegenerative and neuroinflammatory phenotypes under bright-field illumination. In a separate study to be published elsewhere, we will further validate the automatic stereology framework using adjacent sets of sections immunostained for microglia and astrocytes.

2.1. Tissue processing

Aged 6–8 months Tg4510 male mice (n=2) and male non-tg littermate controls (n=2) were selected at random from the colony at the Byrd Alzheimer's Disease Institute at the University of South Florida in Tampa, FL. Mice were deeply anesthetized on an isothermal pad and perfused with 25 ml of cold sterile buffered saline. Brains were removed and one hemisphere immersion fixed for 24h in freshly prepared phosphate buffered paraformaldehyde. After fixation, brains were transferred to Dulbecco's phosphate buffered saline and stored at 4 °C. Prior to sectioning, brains were cryoprotected in 10, 20 and 30% sucrose. Frozen 50-µm sections were collected with a sliding microtome, transferred to 24 well plates in Dulbecco's phosphate buffered saline and stored at 4 °C.

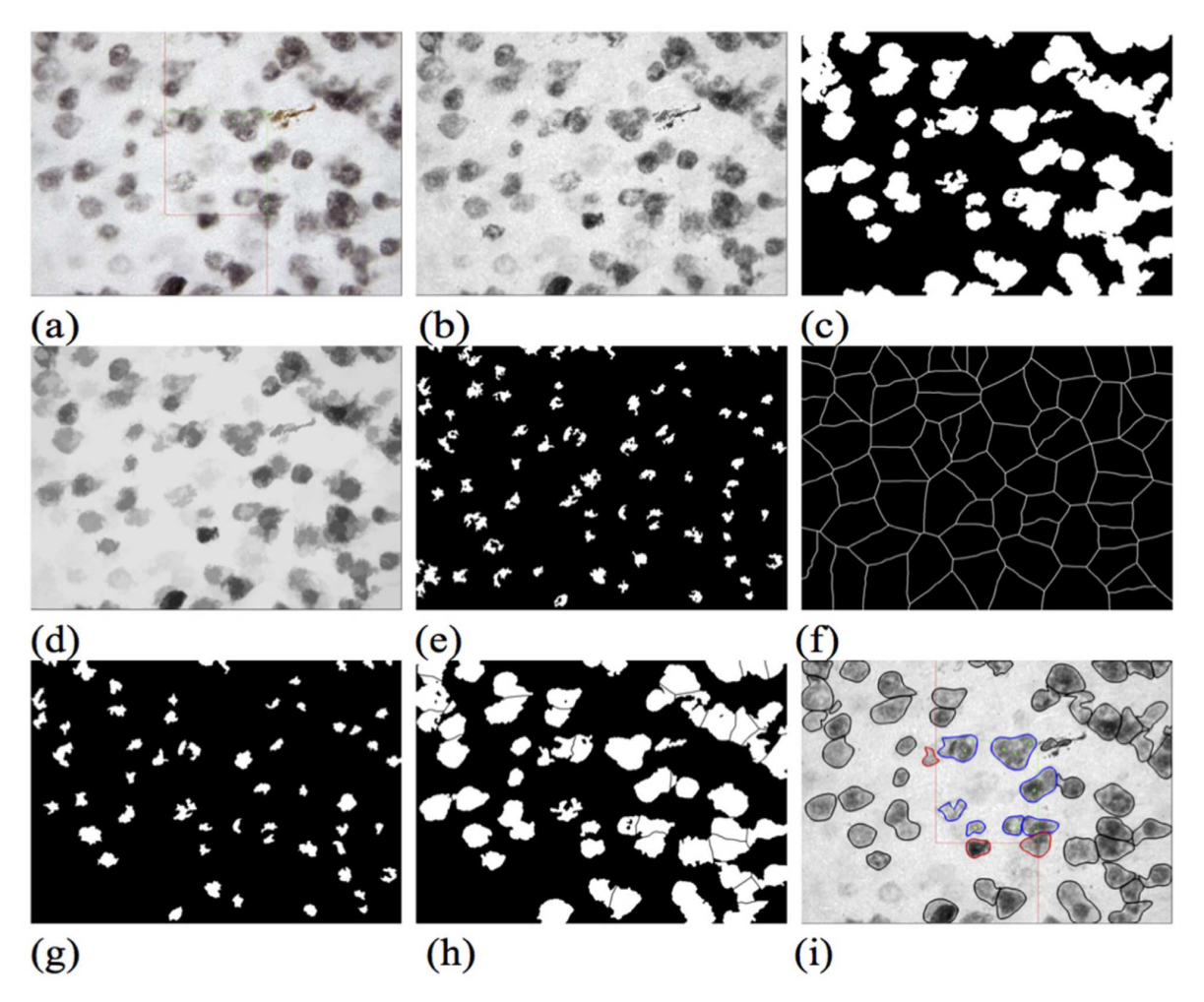


Fig. 1. Intermediate results of different steps in segmentation-stereology approach: (a) original image with manual counts, (b) the EDF image used by the segmentation method, (c) clumps segmented using the threshold computed from estimated GMM, (d) processed EDF image, (e) regional minimas in the processed image, (f) background marker for watershed segmentation, (g) watershed regions reconstructed by regional minimas, (h) Voronoi diagram produced from foreground regions in each segmented clump, (i) final segmentation after smoothing region boundaries by Savitzky-Golay filter. Black regions are removed due to not overlapping with cells of interest, red regions are excluded due to overlapping with exclusion line, and blue regions are neuron targets for automated counting. (For interpretation of the references to colour in this figure legend, the reader is referred to the web version of this article.)

One set of every n^{th} section was sampled in a systematic-random to obtain 6–8 sections through neocortex of each brain.

2.2. NeuN immunostaining

Sections were placed in a multi-sample staining tray and endogenous peroxidase was blocked (10% methanol, 3% H_2O_2 in PBS; 30 min). Tissue samples were permeabilized (with 0.2% lysine, 1% Triton X-100 in PBS solution) and incubated overnight in anti-NeuN (Millipore) primary antibody. Sections were washed in PBS, and then incubated in biotinylated secondary antibody (Vector Laboratories, Burlingame, CA). The tissue was again washed after 2 h and incubated with Vectastain Elite ABC kit (Vector Laboratories, Burlingame, CA) for enzyme conjugation. Finally, sections were stained using 0.05% diaminobenzidine in 0.03% H_2O_2 with nickel intensification. Tissue sections were mounted onto slides, dehydrated, and cover slipped.

2.3. Tissue sampling

Manual counting using the optical fractionator followed by capture-and-save of disector stacks at each location were done using the Stereologer system (Stereology Resource Center, Tampa, FL). The Stereologer software (v10.5) for this system drives the hardware consisting of a Leica DM2500 microscope equipped with low (4x), mid (40x, NA 0.65) and high power (100x, NA 1.3) objectives; NA 1.25 condenser; a motorized X-Y-Z stage (Prior Electronics, Rockland, MA); Sony Firewire DXC-C33 camera; and a Dell PC computer (Windows 10) with i7-4790 CPU and 16 GB of RAM. In practice, there is no need to count all cells in all disectors, only to sample sufficient numbers of disectors in a systematic-random manner to capture most of the within-sample variance (error variance) as measured by the coefficient of error (CE). One mouse (02) was analyzed using manual stereology by both data collectors (C1, C2) to estimate inter-rater variation, which is expected to roughly parallel the error variance.

2.4. Segmentation algorithm

Since cells have arbitrary sizes, shapes, and orientations, none of these features can be assumed a priori by an automatic stereology approach. The segmentation method used in this study was a combination of Gaussian Mixture Model (GMM), morphological operations, watershed segmentation, Voronoi diagrams and boundary smoothing. Fig. 1 presents the visual results of successive steps in the segmentation method on an EDF image. Fig. 1a shows a high optical resolution image (100x, NA 1.3) with the overlaid unbiased disector frame used for manual counts, followed by the EDF image built from a z-stack of images (disector stack) (Fig. 1b). NeuN stained neuronal cell bodies (1 soma = 1 neuron = 1 cell) on the EDF image were segmented by a GMM with two components estimated based on pixel intensities using Expectation Maximization (EM) algorithm. The image was binarized using the threshold computed by a background Gaussian quantile function value and morphological operations followed to extract separate cells (Fig. 1c). Preprocessing of the image by morphological operations with opening by reconstructions followed by closing by reconstructions smoothed the image and removed very small dark or bright cells (Fig. 1d) while connecting very close cells to each other and removing cells below the very small minimas. For watershed segmentation, the image foreground and background markers were extracted with minimas for cells extracted from the preprocessed image (Fig. 1e) and boundaries between cells of a watershed segmentation (Fig. 1f), respectively. The watershed segmentation was applied using the foreground and background markers with foreground cells that overlap the map of segmented cells kept and the others discarded (Fig. 1g). Watershed segmentation expanded original regional minimas and gave a better approximation of boundaries with each cell split using the Voronoi diagrams obtained by the watershed cells inside it (Fig. 1h). In the final step, the cell boundaries were refined using Savitzky-Golay filter (Savitzky and Golay, 1964) which gave smoother boundaries and produced less concave cells. The final segmentation result (Fig. 1i) indicates inclusion (green) and exclusion (red) lines used by the manual and automatic optical fractionator methods. According to the unbiased counting rules for the disector method (Gundersen, 1977), segmented cells were removed that overlapped the exclusion lines of the disector frame. In the final step, the number of NeuN neurons counted in all disector stacks was summed [ΣQ^-] and the total number in neocortex estimated by the optical fractionator formula (Eq. (1)):

Total
$$N_{\text{Neu}} = \left[\sum Q^{-} \right] \bullet F1 \bullet F2 \bullet F3$$
 (1)

where, Total N_{Neu} is the total number of NeuN-immunostained neurons in neocortex; $\sum Q^-$ is the stereology designation for sum of NeuN neurons counted in all disectors; F1 is the reciprocal of the section sampling fraction; F2 is the reciprocal of the area sampling fraction; and F3 is the reciprocal of the thickness sampling fraction.

2.5. Optimal magnification

To assess the optimal magnification for accurate neuron counting, counts of NeuN neurons at low (40x, 0.65) and high (100x oil, NA 1.3) optical resolutions were compared in one non-tg mouse brain. At the first disector location on the first section, NeuN neurons were manually counted using a high-resolution lens (100x, NA 1.3) by thin focal-plan optical scanning with a 10-um high disector. Before moving to the next x-y location, a disector stack of ten z-axis images one micron apart was collected through the first disector volume. This process of manual counting followed by collection of disector stacks was repeated at 200-300 systematic-random x-y locations across all sections at high resolution (100x, NA 1.3), and the entire process repeated using an objective lens with low optical resolution (40x, N.A. 0.65) on the same sections. Disector stacks were used for 1) counting NeuN neurons by the automatic fractionator for comparison with results from the manual fractionator; and, 2) for gold-standard validation (scoring) of manual and automatic fractionator methods by 3-D reconstruction of disector volumes and counting the true number of NeuN neurons.

The results of this pilot study showed both manual and automatic fractionator methods counted more neurons at high

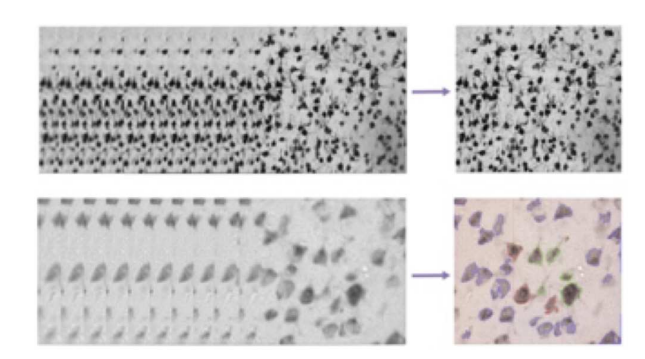


Fig. 2. EDF images (right) created from z-stack of images (left) with low-resolution lens (40x, NA 0.65, upper) and high-resolution lens (100x, NA 1.3, lower). Lower right panel shows disector frame and segmented NeuN neurons counted by the automatic version of the optical fractionator method (West et al., 1991).

optical resolution (Fig. 2, lower) than at low optical resolution (Fig. 2, upper).

Careful 3-D reconstruction of disector stacks confirmed overprojection and masking are the most likely explanations for this consistent underestimation at low optical resolution. As shown in Fig. 3, the high depth of field of the low resolution (40x, NA 0.65) lens prevented adjacent and overlapping cells from being resolved as individual cells (Fig. 3) by either manual or automatic optical fractionator. In contrast, disector stacks collected by high resolution imaging allowed for accurate cell counting, i.e., 98% of NeuN neurons, by both manual and automatic approaches. Finally, this pilot study confirmed that sampling NeuN neurons at 200–300 locations on 6–8 sections generated a sufficiently high level of sampling stringency (CE < 0.05) to reveal group differences for routine neuroscience studies. This work allowed for further validation studies in four genetically modified mouse mice with neurodegeneration as discussed in Section 2.6.

2.6. Validation of automatic optical fractionator

These studies were carried out using NeuN-immunostained sections from 2 Tg4510 mice (Tg-3, Tg-21) and 2 non-tg controls (Ntg-2, Ntg-9) by two technicians with equivalent training and experience. As detailed in Section 2.5, manual fractionator (ground truth) and automatic fractionator counts of NeuN neurons were done in the same disector volumes using high optical resolution (100x, oil immersion, N.A. 1.3) optics. In the first step, manual fractionator counts of neocortical NeuN neurons at each x-y location on each section were followed by collection of disector stacks for estimation of total neuron number using the automatic fractionator. Second, disector stacks were converted to 2-D EDF images with all NeuN-immunostained neurons represented at their maximal plane of focus. Neurons in each EDF image were segmented by the method detailed in Section 2.4. In the final step, the total number of neocortical neurons were estimated in an unbiased manner using the optical fractionator formula [Eq. (1)]. Correlations between separate counts, e.g., manual vs. automatic fractionator, were reported as coefficient of determination (R²). To assess inter-rater variability, two trained technicians counted NeuN neurons through separate sets of optical disectors in the same sections of one mouse neocortex (mouse 02). The average values for two data collectors and two automated counts were used for correlating manual and automatic counts for one mouse (animal 02; Table 1).

3. Results

Table 1 presents correlations between NeuN counts by the automated optical fractionator and ground truth (manual stereology). These results reflect raw counts by two data collectors for a

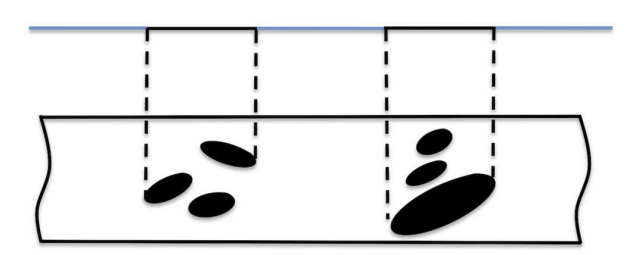


Fig. 3. Schematic of high signal-to-noise objects in a thick section showing over-projection (left) and masking (right). The low-resolution/high depth of field lens causes multiple objects to be counted as one. Hence, a high-resolution lens with low depth of field is required for accurate counts using the manual and automatic optical fractionator.

Table 1NeuN neurons counts by ground truth vs. automatic stereology in n=4 mice. R^2 =correlation for manual and automatic counts.

Mouse ID	Ground Truth	Auto. Count	\mathbb{R}^2
02	1249	1238	>0.96
21	858	878	>0.98
03	570	603	>0.98
09	558	697	>0.98

total of 85 sections from four mice (2 Tg4510, 2 non-tg controls) plus one mouse (C-2) analyzed by both data collectors to assess inter-rater reliability.

The correlations in Table 1 indicate uniformly close relationships between neuron counts by the manual and automatic optical fractionator approaches ($R^2 > 0.96$). Results for counts of NeuNimmunostained neurons in neocortex of Tg4510 mice and non-tg controls are presented in Table 2. Comparison of neocortical neuron counts by the manual and automatic approaches showed a 4% difference for Tg4510 mice and 7% difference for non-tg mice. For the ground truth dataset, there was a 24% difference in neuron number with a slightly higher difference (27%) using the automatic approach. As expected, inter-rater reliability of two data collectors correlated closely to each other ($R^2 = 95\%$, data not shown) at the level expected for the sampling stringency (CE = 0.05). There were no differences in the results for manual versus automatic stereology.

4. Discussion

The optical fractionator method is widely accepted as the current best practice for accurate estimation of total cell number in tissue sections. This rigorous estimator of object number is based on an unbiased design that minimizes or avoids all known sources of stereological and methodological bias. The primary drawback of the manual fractionator is low efficiency (low throughput) due to the requirement for manual cell counting at hundreds of disector locations.

The automatic method proposed here is the first fully automatic segmentation-based approach to incorporate the unbiased principles of the optical fractionator method (Mouton et al., 2016). The approach begins with use of an X-Y-Z motorized stage to automatically collect z-axis stacks of images (disector stacks) at systematic locations in sections sampled through a defined reference volume. Since motorized stage control is a common feature of all commercially available stereology systems, this unbiased sampling approach simply leverages this hardware for capturing disector stacks. In the second step, disector stacks are converted to EDF images in which all cells appear at their maximal plane of focus. Third, a novel algorithm segments stained cells that fall within an unbiased disector frame but do not overlap upper left or bottom exclusion planes. For the segmentation step, we use a novel combination of Gaussian Mixture Models, watershed, and Voronoi diagrams that effectively segmented more than 98% of NeuN neuronal cell bodies in disector stacks (Section 2.5), though it is true that many other algorithms approaches could achieve

Table 2Comparison of ground truth (manual optical fractionator) and the automatic optical fractionator for estimates of total number (±SEM) of NeuN neurons in neocortex of Tg4510 mice and Non-Tg controls.

Group	N	Manual		Automatic		% diff _{NeuN}
		Mean NeuN	SEM _{NeuN}	Mean NeuN	SEM _{NeuN}	
Non-Tg $(n=2)$	2	1.30E + 06	1.18E + 5	1.39E+06	7.71E+04	+7
Tg4510 (n=2)	2	9.81E+05	2.76E + 3	1.02E + 06	1.41E+04	+4
% diff _{NeuN}		-25		-27		

similar results. Since all sampling was carried out in a known fraction of the total reference volume, the final step is to apply the fractionator formula [Eq. (1)] to estimate the total number of cells, without assumptions or considerations about size, shape or orientation.

The approach is demonstrated for automatic counting of high signal: noise (S: N) NeuN-immunostained neurons in neocortex of a transgenic mouse model of tau deposition (Tg4510). Both automatic and manual approaches revealed substantial loss (about 25%) in total number of neocortical NeuN neurons in brains of Tg4510 mice at 6-8 months of age compared to non-tg controls as reported previously in these mice of the same age using manual stereology (Spires et al., 2006). Analysis of the same disector

volumes showed a strong correlation ($R^2 > 0.96$) between the automatic and manual versions of the optical fractionator, which was closely comparable to the correlation of two human collectors to each other ($R^2 = 95\%$). Thus, these results confirm comparable accuracy of counting of NeuN neurons by the automatic approach with similar precision (reproducibility; $R^2 = 96\%$) as manual counts by two data collectors.

Using results from gold-standard counts, the results from ground truth (manual) and automatic fractionator methods could be scored for accuracy. Furthermore, these 3-D reconstruction counts allowed for identification of the precise reasons for mismatches (residual variation) between manual and automatic counts. Fig. 4 shows NeuN neuron counts by section for manual

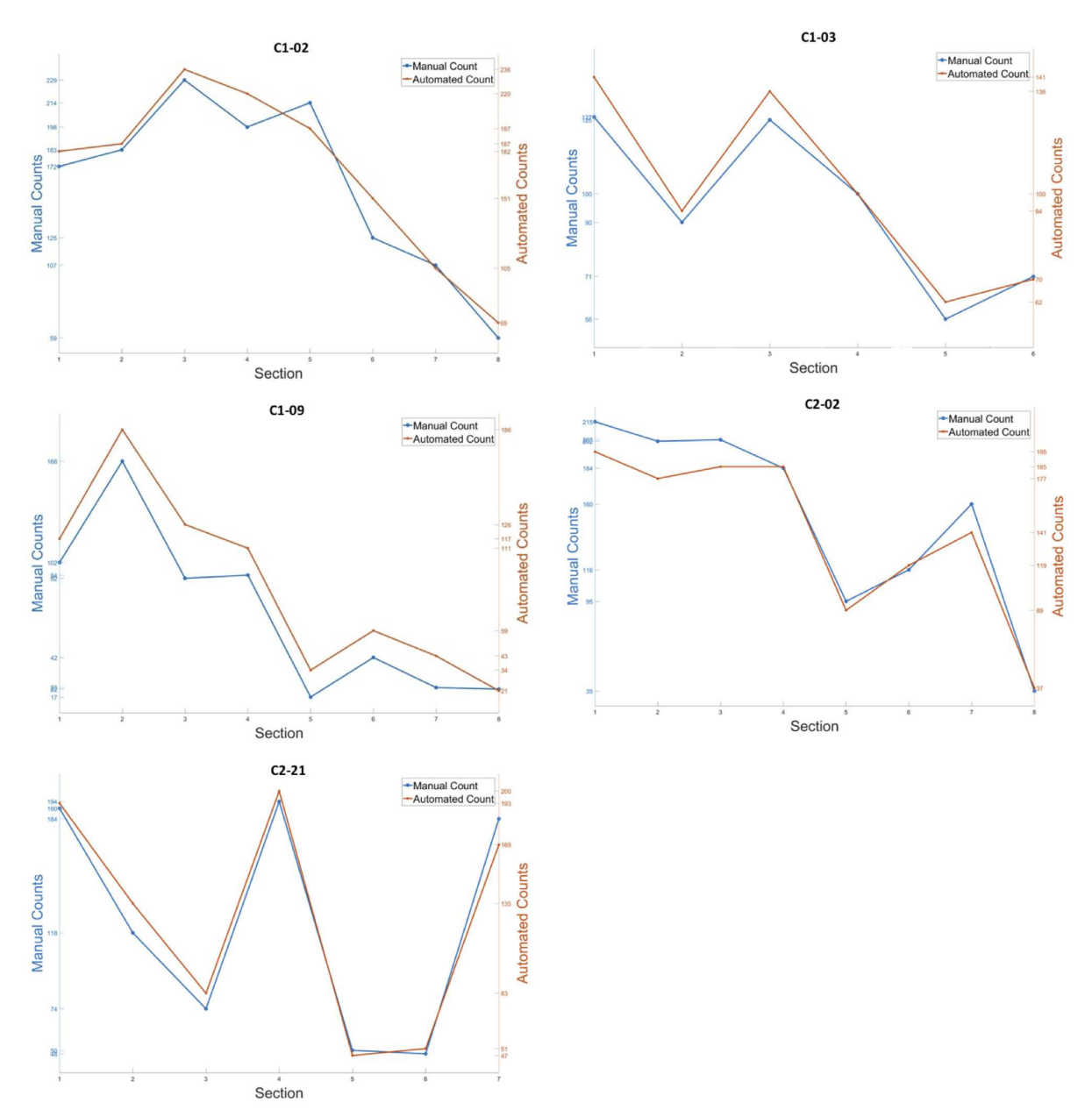


Fig. 4. Plots of manual and automated counts of different sections for 4 cases. These plots of Neu-N neuron counts by section show the relative agreement between the objective automated framework and subjective manual counts by 2 data collectors (C1 and C2). The residual errors in these correlations arise from both approaches. (For interpretation of the references to colour in the text, the reader is referred to the web version of this article.)

and automated approaches for each of the comparisons in Table 2. These plots show the relative overlap of manual counts by two data collectors (blue) versus automatic counts in the same disector volumes (red). Since the two data collectors for mouse 02 were carried out at separate disector locations, these plots show nonoverlapping counts across the same sections [Fig. 4, plots (a) and (d)]. The first observation is that total cell counting errors by manual and automatic methods occur in less than 5% of disector volumes, or about 4 or 5 mismatches per 100 disectors. As expected from our previous automatic algorithms to detect stained cells on tissue sections (Mouton et al., 2005; Chaudhury et al., 2013; Phoulady et al., 2015, 2016a, 2016b) most residual variance in the correlations of ground truth (manual) and automatic counts was due to the manual data collection. Three-dimensional reconstruction of disector stacks showed more frequent errors by the manual counting (~3-4 mismatches per 100 disector stacks) than by the automatic approach (\sim 1–2 errors per 100 disector stacks) with most manual counting errors leading to underestimation (false negatives), e.g., Sections 1-7 in Fig. 4(c). Specifically, 3-D reconstructions of disector stacks for these mismatches showed the human data collector failed to resolve overlapping neurons in the z-axis. These errors due to the high depth of field (low resolution) of the 40x lens (Fig. 3, Section 2.5) could be minimized by a higher numerical aperture 40x objective. In contrast, underestimates at high resolution can be minimized by slower focusing through the z-axis at each disector location. Careful 3-D reconstruction of disector stacks showed the second most common source of mismatches by manual stereology was false positives where the data collector incorrectly counted cells touching exclusion planes. Thus, the manual optical fractionator method could in theory attain an equivalent accuracy of the automatic approach, provided time is taken to carefully focus through each disector volume. The caveat is that this process further reduces the efficiency of conventional cell counting using the manual optical fractionator.

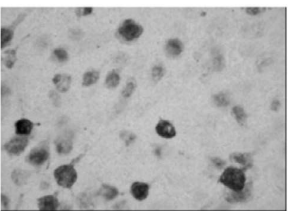
For the automatic approach, converting disector stacks to EDF images allowed for clear separation and segmentation of each NeuN neuron at its optimal plane of focus, thereby allowing the algorithm to resolve the correct number of overlapping cells in the z-axis. Pixel-level resolution of exclusion planes and cell boundaries eliminated errors at the exclusion planes. Except for a few parameters, e.g., minima and maxima, most of the parameters in the segmentation algorithm were set in an automatic and adaptive manner separately for each image, making the automatic framework resistant to variations in image acquisition. For instance, because images collected in the dataset had varying brightness, intensity thresholds were set adaptively by the estimated GMM for each image, allowing the algorithm to generate consistent segmentations for different cell types, staining intensities and microscope settings that vary brightness at the image and neuron levels under bright-field illumination (Fig. 5).

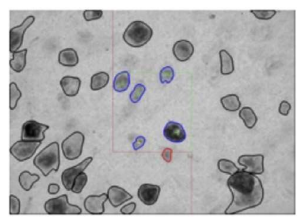
It is worth reiterating that only 1–2 errors per 100 disectors occurred during automatic counting of NeuN neurons in disector stacks. In most of these cases, 3–D reconstruction indicated the

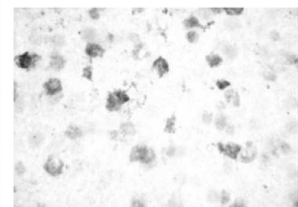
automatic algorithm counted fewer NeuN neurons than the true number, e.g., Fig. 4(f), Sections 1-3. The most likely explanation for these mismatches are (a) one neuron minima is not detected; (b) two overlapping neurons are not split because the size is less than the maximum threshold; or (c) the solidity of the neuron obtained by the refined boundary of original neuron is larger than the average solidity of all neurons. These mismatches tended to occur in areas with highly crowded cells and very low contrast, as was the case for underestimate errors by manual cell counting. In a few rare cases, the automatic algorithm failed to split multiple cells leading to a false positive, or the algorithm detected a staining artifact. Further segmentation optimization will minimize mismatches by pre-processing to remove artifacts and post-processing to merge close regions (avoid split cells). Another practical step to further improve the automatic optical fractionator is optimization of immunostaining protocols to increase S: N and avoid staining artifacts.

Beside equal or superior accuracy and precision to manual cell counting, two advantages of the automatic optical fractionator are 8-fold higher throughput efficiency and 100% objectivity as compared to manual cell counting. Though this work compared the proposed automatic framework with manual counting using just one commercially available stereology system, all current systems use essentially the same hardware technology and manual cell counting approaches. All these systems require about 20-30 min to delineate reference areas and compute results, and 3-4 h to achieve a CE of 0.05 by manual thin-focal plane optical scanning and counting (clicking) on stained cells in about 200-300 optical disectors across 6-8 sections. This level of sampling rigor is typically sufficient to show significant group differences down to about 15%, or demonstrate significant differences do not exist without risking a Type 2 statistical error. To achieve the same level of accuracy and sampling stringency, the automatic stereology framework (ASF, Fig. 6) required an average of about 30 min per case, including 6-8 min to manually delineate reference spaces at low power; 10-12 min to automatically capture and save disector stacks to random access memory; and 8-10 min to create EDF images, run the segmentation algorithm, and compute the total number of neurons.

A survey of segmentation algorithms proposed to improve efficiency of cell counting methods show these segmentation approaches focus on finding number of 2-D cell profiles (Sjöström et al., 1999; Nattkemper et al., 2001; Ray et al., 2002; Benali et al., 2003; Peng et al., 2003; Lin et al., 2005; Long et al., 2005, 2006; Costa and Bollt 2006; Inglis et al., 2008; Ho et al., 2011; Liu et al., 2014; de Gracia et al., 2015). Per the Delesse principle (1847), the total number of arbitrary 3-D cells on tissue sections is not equal to the total number of their 2-D profiles, i.e., Total $N_{\text{cells}} \neq \text{Total}$ N_{profiles} . Though automatic and therefore rapid, current automatic segmentation approaches are biased by failure to count in 3-D, reliance on cell densities (Reference Trap), use of faulty correction factors, and other assumption- and model-based morphometry (Gundersen et al., 1988; Mouton, 2016), and therefore lack the robustness required for bioscience research.







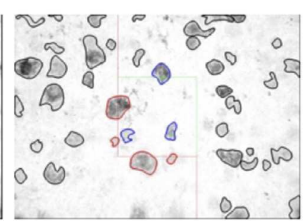


Fig. 5. Two EDF images with variable brightness [left (a) and (b)] and the same images after segmentation [right (a) and (b)].

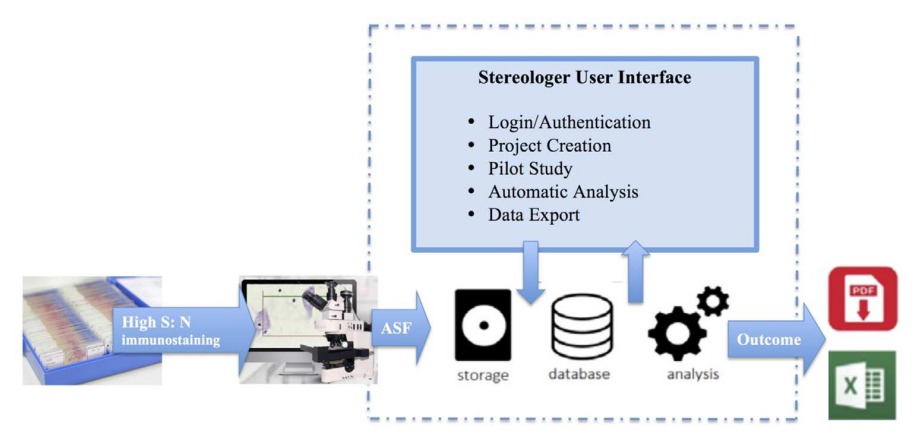


Fig. 6. Schematic diagram of the proposed ASF workflow.

Another factor that limits the accuracy of previous approaches is the often ignored prerequisite that accurate use of the optical fractionator method requires a thin focal plane for optical scanning in the z-axis. A pilot study to assess optimal magnification for these studies provided empirical evidence that low resolution optics causes systematic underestimation of counts due to over-projection and masking. These factors could be practically eliminated at high resolution by applying a modified segmentation algorithm with advanced post-processing steps, e.g., using a classifier to indicate likely split or overlapping neurons. For the automatic and manual counts at low resolution, a similar strategy would not resolve the correct number of cells because the high depth of field of standard low resolution lenses effectively collapse cells onto a single observation plane. A second argument in favor of high resolution optics for both manual and automatic fractionator methods is that both approaches require thin focal plane scanning through the z-axis to determine the section thickness, i.e., difference in linear distance between the upper and lower optical planes of each section (Elozory et al., 2012). Accurate identification of section thickness by high optical resolution is required for accurate calculation of the thickness sampling fraction (tsf; see Eq. (1)). Though we only compared optical resolution using one low (40x, NA 0.65) and one high (100x oil, NA oil) lens in this study. it is expected that other high resolution lenses with thin focal planes such as 63x oil (NA 1.3) would give comparable accuracy.

A further application of the present automatic stereology framework is that the mean cell (soma) volume and true size distribution (Gundersen et al., 1988; Jensen and Gundersen, 1993; Mouton et al., 2015). These size parameters can be determined from the cell boundaries at their maximum focal plane on EDF images without additional labor or images, and only negligible increase in computation time. In contrast, estimating mean cell size by manual stereology more than doubles the time and effort over estimation of cell number alone. Future directions to improve efficiency include automatic delineation of reference spaces by pattern recognition at low power, and high performance computing, i.e., increased number of cores, for parallelization of EDF image creation and algorithm computations.

5. Conclusions

The proposed automatic, objective and accurate optical fractionator method achieves a dramatic improvement in throughput efficiency over the current manual optical fractionator. The automatic approach is 100% objective and not subject to the subjective human errors that reduce accuracy including false negatives from overlapping cells, false positives from cells

overlapping with exclusion planes, inter-rater bias, recognition errors and user fatigue. This automatic stereology approach will be useful for a wide range of bioscience studies, and especially those with large workloads that are currently inaccessible to unbiased stereology methods.

Acknowledgments

The authors would like to acknowledge funding support from Small Business Innovative Research (SBIR) grants to PRM from the U.S. Public Health Service (NIH), grants to PRM and DG from the Florida High Technology Corridor program, and a grant to PRM from the Byrd Alzheimer's Institute at the University of South Florida, Tampa, FL. The authors thank Raj Patel and Robert D. Elkins for manual cell counting for these studies.

References

Benali, A., Leefken, I., Eysel, U.T., Weiler, E., 2003. A computerized image analysis system for quantitative analysis of cells in histological brain sections. J.

Neurosci. Methods 125 (1), 33–43.
Bradley, A.P., Bamford, P.C., 2004. A one-pass extended depth of field algorithm based on the over-complete discrete wavelet transform. Image Vision Comput. '04 N. Z. 279–284.

Chaudhury, B., Phoulady, H.A., Goldgof, D., Hall, L.O., Mouton, P.R., Hakam, A., Siegel, E.M., 2013. An ensemble algorithm framework for automated stereology of cervical cancer. International Conference on Image Analysis and Processing, Springer, Berlin Heidelberg, pp. 823–832.

dCosta, L. da F., Bollt, E., 2006. Fast and accurate nonlinear spectral method for image recognition and registration. Appl. Phys. Lett. 89 (17), 174102.

Delesse, M.A., 1847. Procede mecanique pour determiner la composition des roches. C. R. Acad. Sci. Paris 25, 544–545.

Elozory, D.T., Kramer, K.A., Chaudhury, B., Bonam, O.P., Goldgof, D.B., Hall, L.O., Mouton, P.R., 2012. Automatic section thickness determination using an absolute gradient focus function. J. Microsc. 248 (3), 245–259.

Gundersen, H.J.G., Bagger, P., Bendtsen, T.F., Evans, S.M., Korbo, L.X.M.N., Marcussen, N., Sorensen, F.B., 1988. The new stereological tools: disector, fractionator, nucleator and point sampled intercepts and their use in pathological research and diagnosis. APMIS 96 (7–12), 857–881.

Gundersen, H.J.G., 1977. Notes on the estimation of the numerical density of arbitrary profiles: the edge effect. J. Microsc. 111 (2), 219–223. Ho, S.Y., Chao, C.Y., Huang, H.L., Chiu, T.W., Charoenkwan, P., Hwang, E., 2011.

Ho, S.Y., Chao, C.Y., Huang, H.L., Chiu, T.W., Charoenkwan, P., Hwang, E., 2011. NeurphologyJ: an automatic neuronal morphology quantification method and its application in pharmacological discovery. BMC Bioinf. 12 (1), 1.

Inglis, A., Cruz, L., Roe, D.L., Stanley, H.E., Rosene, D.L., Urbanc, B., 2008. Automated identification of neurons and their locations. J. Microsc. 230 (3), 339–352.
Jensen, E.V., Gundersen, H.J.G., 1993. The rotator. J. Microsc. 170 (1), 35–44.

Jensen, E.V., Gundersen, H.J.G., 1995. The rotator. J. Microsc. 170 (1), 35–44.
Lin, G., Chawla, M.K., Olson, K., Guzowski, J.F., Barnes, C.A., Roysam, B., 2005.
Hierarchical, model-based merging of multiple fragments for improved three-dimensional segmentation of nuclei. Cytom. Part A 63 (1), 20–33.

Liu, J.Y., Ellis, M., Brooke-Ball, H., de Tisi, J., Eriksson, S.H., Brandner, S., Thom, M., 2014. High-throughput, automated quantification of white matter neurons in mild malformation of cortical development in epilepsy. Acta Neuropathol. Commun. 2 (1), 1.

Long, X., Cleveland, W.L., Yao, Y.L., 2005. A new preprocessing approach for cell recognition. IEEE Trans. Inf. Technol. Biomed. 9 (3), 407–412.

- Long, X., Cleveland, L., Yao, Y.L., 2006. Automatic detection of unstained viable cells in bright field images using a support vector machine with an improved training procedure. Comput. Biol. Med. 36 (4), 339–362.
 Mouton, P.R., Durgavich, J., Ingram, D.K., 2005. Automatic estimation of size
- Mouton, P.R., Durgavich, J., Ingram, D.K., 2005. Automatic estimation of size parameters using verified computerized stereoanalysis. Image Anal. Stereol. 24 (1), 41–49.
- Mouton, P.R., Phoulady, H.A., Goldgof, D., Hall, L.O., Siegel, E., 2015. Automatic stereology of substantia nigra using a novel segmentation framework based on the balloon active contour model. Soc. Neurosci. 735.08, Chicago, IL.
- Mouton, P.R., Phoulady, H.A., Goldgof, D., Hall, L.O., Gordon, M., Patel, R., Elkins, R.D., Morgan, D., 2016. Tg4510 mice provide an effective model for testing neuroprotective therapies in early stage Alzheimer's disease. Soc. Neurosci. 767.08. San Diego.
- Mouton, P.R., 2016. Quantitative anatomy using unbiased stereology. In: Neu, Corey P., Genin, Guy M. (Eds.), CRC Handbook of Imaging in Biological Mechanics. CRC Press, London 579 pp., October 23, 2014.
- Nattkemper, T.W., Ritter, H.J., Schubert, W., 2001. A neural classifier enabling high-throughput topological analysis of lymphocytes in tissue sections. IEEE Trans. Inf. Technol. Biomed. 5 (2), 138–149.
- Peng, S., Urbanc, B., Cruz, L., Hyman, B.T., Stanley, H.E., 2003. Neuron recognition by parallel potts segmentation. Proc. Natl. Acad. Sci. 100 (7), 3847–3852.
- Phoulady, H.A., Goldgof, D., Hall, L., Mouton, P.R., 2015. An approach for overlapping cell segmentation in multi-layer cervical cell volumes. First place overlapping cervical cytology image segmentation challenge. International Society for Biomedical Imaging (IEEE), Brooklyn, NY.
- Phoulady, H.A., Goldgof, D.B., Hall, L.O., Mouton, P.R., 2016a. Histopathology image segmentation with hierarchical multilevel thresholding. Proceedings of the SPIE Medical Imaging On Digital Pathology, San Diego, CA.

- Phoulady, H.A., Goldgof, D.B., Hall, L.O., Mouton, P.R., 2016b. A new approach to detect and segment overlapping cells in multi-layer cervical cell volume images. Proceedings Of The International Symposium On Biomedical Imaging (ISBI), Prague, Czech Republic.
- Ray, N., Acton, S.T., Ley, K., 2002. Tracking leukocytes in vivo with shape and size constrained active contours. IEEE Trans. Med. Imaging 21 (10), 1222–1235.
 SantaCruz, K., Lewis, J., Spires, T., Paulson, J., Kotilinek, L., Ingelsson, M., Forster, C.,
- SantaCruz, K., Lewis, J., Spires, T., Paulson, J., Kotilinek, L., Ingelsson, M., Forster, C., 2005. Tau suppression in a neurodegenerative mouse model improves memory function. Science 309 (5733), 476–481.
- Savitzky, A., Golay, M.J., 1964. Smoothing and differentiation of data by simplified least squares procedures. Anal. Chem. 36 (8), 1627–1639.
- Sjöström, P.J., Frydel, B.R., Wahlberg, L.U., 1999. Artificial neural network-aided image analysis system for cell counting. Cytometry 36, 18–26.Spires, T.L., Orne, J.D., SantaCruz, K., Pitstick, R., Carlson, G.A., Ashe, K.H., Hyman, B.T.,
- Spires, T.L., Orne, J.D., SantaCruz, K., Pitstick, R., Carlson, G.A., Ashe, K.H., Hyman, B.T., 2006. Region-specific dissociation of neuronal loss and neurofibrillary pathology in a mouse model of tauopathy. Am. J. Pathol. 168 (5), 1598–1607.
- pathology in a mouse model of tauopathy. Am. J. Pathol. 168 (5), 1598–1607. Sterio, D.C., 1984. The unbiased estimation of number and sizes of arbitrary particles using the disector. J. Microsc. 134 (2), 127–136.
- Valdecasas, A.G., Marshall, D., Becerra, J.M., Terrero, J.J., 2001. On the extended depth of focus algorithms for bright field microscopy. Micron 32 (6), 559–569.
- West, M.J., Slomianka, L.H.J.G., Gundersen, H.J.G., 1991. Unbiased stereological estimation of the total number of neurons in the subdivisions of the rat hippocampus using the optical fractionator. Anat. Rec. 231 (4), 482–497.
- Wicksell, S.D., 1925. The corpuscle problem: a mathematical study of a biometric problem. Biometrika 84–99.
- de Gracia, P., Gallego, B.I., Rojas, B., Ramirez, A.I., de Hoz, R., Salazar, J.J., Ramirez, J.M., 2015. Automatic counting of microglial cells in healthy and glaucomatous mouse retinas. PLoS One 10 (11), e0143278.